

A continuous stream flash evaporator for the calibration of an IR cavity ring down spectrometer for isotopic analysis of water

V. Gkinis¹, T. J. Popp¹, S. J. Johnsen¹, and T. Blunier¹

¹Centre for Ice and Climate, Niels Bohr Institute, University of Copenhagen, Juliane Maries Vej 30, DK-2100 Copenhagen, Denmark

I. ABSTRACT

A new technique for high resolution simultaneous isotopic analysis of $\delta^{18}\text{O}$ and δD in liquid water is presented. A continuous stream flash evaporator has been designed that is able to vaporise a stream of liquid water in a continuous mode and deliver a stable and finely controlled water vapour sample to a commercially available Infra Red Cavity Ring Down Spectrometer.

Injection of sub μl amounts of the liquid water is achieved by pumping liquid water sample through a fused silica capillary and instantaneously vaporizing it with a 100% efficiency in a home made oven at a temperature of 170°C . The system's simplicity, low power consumption and low dead volume together with the possibility for automated unattended operation, provides a solution for the calibration of laser instruments performing isotopic analysis of water vapour. Our work is mainly driven by the possibility to perform high resolution on line water isotopic analysis on Continuous Flow Analysis systems typically used to analyze the chemical composition of ice cores drilled in polar regions. In the following we describe the system's precision and stability, sensitivity to varying levels of sample size and we assess the observed memory effects. A test run with standard waters of different isotopic composition is presented, demonstrating the ability to calibrate the spectrometer's measurements on a VSMOW scale with a relatively simple and fast procedure.

II. INTRODUCTION

High precision stable isotope analysis of water is typically performed offline via discrete sampling with traditional isotope ratio mass spectrometry (hereafter IRMS). While high precision and accuracy can routinely be achieved with IRMS systems, water isotope analysis remains an elaborate process, which is demanding in

terms of sample preparation, power consumption, sample size, consumable standards, and carrier gases.

In the most common IRMS techniques, water molecules are not measured as such, but are converted to a different gas prior to measurement. For $\delta^{18}\text{O}$ analysis, the CO_2 equilibration method (1) has been widely used, whereas δD analysis commonly involves the reduction of water to hydrogen gas over hot uranium (2; 3) or chromium (4).

However, combined use of these methods rules out simultaneous analysis of both water isotopologues on a given sample. More recently, in combination with continuous flow mass spectrometers, conversion of water to CO and H_2 is performed in a pyrolysis furnace (5; 6) and allows simultaneous measurement, but still on a discrete sample.

Laser spectroscopy at the near and mid infrared regions has been demonstrated as a potential alternative for water isotope analysis, presenting numerous advantages over IRMS (7; 8). A major advantage of the technique is the ability to directly inject the sampled water vapour in the optical cavity of the spectrometer where both isotopic ratios $^{18}\text{O}/^{16}\text{O}$ and $^2\text{H}/^1\text{H}$ are simultaneously measured. Nowadays, commercial IR spectrometers are available with a precision comparable to IRMS systems (9; 10). These units typically receive a continuous stream of water vapour sample and offer ease of use and portability.

The problem of the calibration of an IR spectrometer for isotopic analysis of water vapour has been addressed in the past by other studies. Wang et al (11) calibrated an IR - spectrometer in an Off - Axis Integrated Cavity Output (OA - ICOS) configuration by monitoring the differences between a measured and a theoretically predicted Rayleigh distillation curve. In order to obtain a saturated gas stream they make use of a dew point generator. This approach requires precise measurement

of the total time of the Rayleigh distillation process. The initial and final masses of the liquid water standard used, also need to be measured. The time required for the process to complete depends on the required precision and is of the order of 12-24 hours.

A different approach to the problem, is the generation of water vapour with known isotopic composition, by introducing liquid water standards in a dry gas stream, preferably at high temperatures. In this case, immediate 100% evaporation is essential in order to avoid isotopic fractionation effects. Proper control of the injected amount of liquid water and the dry gas flow is essential for a stable water mixing ratio, while it can in principle allow for tuning of the system to different humidity levels. A dripper device, used by Lee et al (12) introduced liquid water in a heated evaporation chamber filled with high purity nitrogen. The device operates in the range 800-30,000 ppm and delivers water vapour sample to a direction absorption spectrometer operating in the mid IR region ($6.66 \mu m$). Iannone et al (13), use a piezoelectric microdroplet generator (14) in order to inject sub μl amounts of water in a stream of dry gas where 100% evaporation takes place. The sample is then forwarded to a V-shaped high reflectivity cavity in an Optical Feedback - Cavity Enhanced Absorption Spectroscopy (OF-CEAS) configuration (15; 16). Aiming for in situ isotopic analysis of water vapour in the Upper Troposphere - Lower Stratosphere region where water mixing ratios are extremely low, the latter system is optimised in the range between 12 and 3500 ppm. Both evaporation systems use a relatively large volume, (order of mL) static liquid water reservoir as a sample (or standard) source.

The motivation of this study lies in the area of ice core research with the goal to develop a system that can perform on line δD and $\delta^{18}O$ isotopic analysis on a liquid sample stream originating from a continuously melting ice rod. Similar melting systems have been developed and used in lab or field environments for the analysis of chemical impurities or gases entrapped in the ice core (17; 18; 19). In this way, it is possible to perform measurements with high resolution when compared to equivalent measurements performed on discrete samples. Portability, low power consumption and cost have been parameters that were considered for this system.

III. EXPERIMENTAL

A. NIR Cavity Ring Down Spectroscopy

Water molecules present spectral absorption lines in the area of mid and near infra red due to ro-vibrational (fundamental and overtone) transitions. At low sample

pressures, the absorption lines are narrow enough to permit distinction between different isotopologues. These spectral features are unique and their relative intensities can be linked to relative isotopic abundances, hence providing the necessary information to calculate isotopic ratios. For a comprehensive description on the various optical techniques and analysis of the signals in IR spectroscopy as applied for isotopic analysis, the reader may refer to (20). In this study we use a commercial IR spectrometer purchased from Picarro Inc. ($L1102 - i$) (21). For high signal to noise ratio at a relatively low water concentration, the spectrometer utilizes a high finesse cavity in a Cavity Ring Down (CRDS) configuration (22). In a typical CRDS experiment the laser light is coupled into the optical cavity and stays in resonance until the intensity builds up to a maximum value. The light source is then turned off and the light intensity in the cavity decays exponentially as photons “leak” through the mirrors of finite reflectivity. The result is that every photon completes thousands of roundtrips in the cavity, thus interacting with the injected absorbing sample through a path length of the order of kilometers. The time constant of this decay, commonly referred to as “ring down time”, depends only on the reflectivity of the mirrors \mathcal{R} , the length of the cavity l_c and the absorption coefficient of the selected absorption feature $\alpha(\nu)$ (23). The ring down time is described in Eq. 1. Absorption spectra can thus be derived by the measurement of τ at different emission wavenumbers ν .

$$\tau(\nu) = \frac{l_c}{c[(1 - \mathcal{R}) + \alpha(\nu)l_c]} \quad (1)$$

In our system the IR spectrometer operates in a continuous flow-through mode, maintaining a cavity pressure of 35 Torr at a gas sample flow rate of $\approx 30 \text{ mL/min}$ at STP via two PID controlled proportional valves up and downstream of the optical cavity. The temperature of the cavity is regulated at 80°C . The acquisition rate of the instrument is one data point in ≈ 6 seconds.

B. Sample preparation

We implement a continuous liquid water stable isotope analysis by converting a stream of liquid water to water vapour and thereafter introducing the latter into the optical cavity of a NIR-CRDS spectrometer. A sketch of the system is given in figure 1. Different liquid water samples (or standards) can be selected via a 6 port selection valve (V1). Transfer of the sample is done using a peristaltic pump that maintains a liquid flow rate of 0.1 mL/min over the sample line. This flow rate can be adjusted according to the needs of the application or

potential sample limitations. High purity Perfluoroalkoxy (PFA) tubing with an ID of 0.5 mm is used in this section.

A water level in the range of 17,000 - 22,000 ppmv in the optical cavity results in optimum spectrometer performance. With a nominal gas flow rate of 30 mL/min STP and a concentration of 20,000 ppmv the required injection rate is $\approx 0.5 \mu\text{L}/\text{min}$ of liquid water. In order to introduce this- quantity of liquid water in the oven, we split off a fraction of the main sample line through a fused silica capillary. The split takes place in a PEEK Tee split with $\varnothing 0.5$ mm bore (T1 in figure 1).

The small ID of the capillary tube acts as a restriction that imposes a back pressure at T1. In order to balance the capillary back pressure we apply a restriction on the waste line downstream of the T1 Tee by using tubing with an ID smaller than the $\varnothing 0.5$ mm of the main sample line. Assuming laminar flow, an estimate of the pressure build up along a tube is given by the Hagen-Poiseuille law as described in Eq. 2.

$$\Delta p = \frac{8\eta L Q^4}{\pi r} \quad (2)$$

Where Δp is the pressure drop along a tube with length L and inner diameter $2r$ and Q is the volumetric flow rate of the fluid with dynamic viscosity η .

Proper selection of length and inner diameter for the waste line and capillary tubes balances the two back pressures and offers a way to tune the flow rates through the capillary. At steady state the flow through the capillary (Q_c) will be

$$Q_c = Q_w \frac{L_w r_c^4}{L_c r_w^4} \approx Q_m \frac{L_w r_c^4}{L_c r_w^4} \quad (3)$$

where Q_w and Q_m the flow of liquid sample at the waste and main line respectively. Due to the strong dependance of Q_c on the inner diameter α of the tubes, the latter serve as a first order control on the flow through the capillary. Typical values for α_c and α_w are 20 μm and 150 μm respectively. Considering a fixed value for the length of the capillary L_c ($L_{cap} = 15\text{cm}$), the linear dependance of Q_c on Q_m and L_w allows for fine tuning of the flow by varying the length of the tube at the waste line and the flow rate on the peristaltic pump. A detailed view on the liquid sample handling and the tubing sizes involved is presented in figure 2.

The sample evaporation step is critical as 100% immediate evaporation is essential in order to avoid isotopic fractionation effects. The evaporation oven consists of a stainless steel Valco Tee-split (Valco ZT1M) (T2 in figure 1), attached on top of an aluminum block measuring $40 \times 40 \times 30$ mm. The bore space in the

Tee-split ($\varnothing 0.5$ mm) serves as the evaporation chamber. We maintain a temperature of 170 °C by means of a PID controlled 200 W cartridge heater (Omega CSH-201200) fixed in the aluminum block. A temperature reading is obtained with a K type thermocouple. High temperature conductive paste is used in all of the connections of the evaporation chamber to ensure optimal heat distribution. Upon evaporation of the liquid sample in the oven, mixing with dry air takes place, forming the gas sample with the desired water vapour levels. Atmospheric air is dried through a TMDrierite canister (CaSO_4). Typical water levels for the dry gas are below 100 ppm water concentration. For the transfer of dry gas to the evaporation chamber we use stainless steel 1/16" diameter tube. The mixture of dry gas and water vapor is transferred to the spectrometer at the nominal flow rate of 30 cc/min via a 1/16" stainless steel tube that is heated to $\approx 90^\circ\text{C}$ in order to avoid recondensation of water vapour on the walls of the tube.

Overall our approach is towards minimizing dead volume in the system, thus reducing sample dispersion and limiting memory effects, while at the same time we ensure efficient evaporation and negligible fractionation of the water sample.

IV. RESULTS AND DISCUSSION

A. System Stability - Allan Variance

We investigate the behavior of the spectrometer in combination with the sample preparation system, regarding possible instrumental drift during long operation. Injection of de-ionised water from a 5-liter bottle takes place for a period of ≈ 16 hours. The level of water vapour in the cavity during this period is 19510 ± 154 ppm [1σ]. Results of the test are presented in figure 3. This test was performed with an acquisition rate of ≈ 1 data point every 6 sec. In a second stage we set the data on a fixed time step of 6 sec by means of linear interpolation.

We perform a "clean-up" of the raw data by removing outliers that deviate more than $\pm 3\sigma$ from the mean value of the run. For a total of 9551 points, we rejected 17 and 5 outliers for $\delta^{18}\text{O}$ and δD respectively. We observe that extreme outliers are likely to occur during sudden and short term interruption of the water sample delivery. Small bubbles or other impurities in the water stream are likely to cause such effects. Noisy and frequently interrupted delivery of sample to the spectrometer can deteriorate the measuring performance of the system.

Assuming that data points are normally distributed then a mean and variance for this distribution are defined as:

$$\bar{\delta} = \frac{1}{N} \sum_{i=1}^N \delta_i \quad (4)$$

$$\sigma_{\delta}^2 = \frac{1}{N-1} \sum_{i=1}^N (\delta_i - \bar{\delta})^2 \quad (5)$$

For sample size N the standard error of the mean can be calculated as:

$$\sigma_{\bar{\delta}}^2 = \left(\frac{\partial \bar{\delta}}{\partial \delta} \sigma_{\delta} \right)^2 = \frac{1}{N} \sigma_{\delta}^2 \quad (6)$$

Equation 6 implies that in the theoretical case of a zero drift system, one can progressively decrease the standard deviation of the mean by increasing the integration time of the measurement. However, apparent instrumental drifts are bound to limit the benefits of averaging a signal over long integration times.

In order to assess the stability of the system we follow an approach similar to (24) and (25) by calculating the Allan variance (26) for the time series presented in figure 3. A time series of sample size N can be divided in m subsets of sample size $k = \frac{N}{m}$. If the acquisition time per data point is t_i then the integration time for every subset is $\tau_m = kt_i$. The Allan variance can then be defined as:

$$\sigma_{Allan}^2(\tau_m) = \frac{1}{2m} \sum_{j=1}^m (\bar{\delta}_{j+1} - \bar{\delta}_j)^2 \quad (7)$$

where $\bar{\delta}_{j+1}$ and $\bar{\delta}_j$ are the mean values of neighboring intervals j and $j+1$.

In figure 4 we plot the calculated Allan variance with different integration times for $\delta^{18}\text{O}$ and δD . For integration times up to about $\tau_{opt} = 5000$ sec the Allan variance decreases linearly for both isotopologues. This linear behavior suggests a white noise signal and further averaging can lead to an improvement in the detection level of the system. However for integration times longer than τ_{opt} averaging is not expected to improve the detection levels any further due to apparent instrumental drifts. Practically, for the purpose of calibration it is unlikely that averaging times longer than ≈ 600 sec will be implemented. As a result the optimum performance of the system at τ_{opt} is not fully exploited. However the value of τ_{opt} for both $\delta^{18}\text{O}$ and δD indicates a stable performance for both the spectrometer and the sample preparation line with a precision comparable or better to mass spectrometry systems used for $\delta^{18}\text{O}$ and δD isotopic analysis. This behavior is due to the optimized control of the spectrometer's cavity temperature and pressure and the smooth and finely controlled evaporation and delivery of the water vapour sample.

B. Dependence on humidity levels

We investigate the response of the system to different levels of injected water sample. The pump rates of P1 are tuned in subsequent steps to 13 different humidity levels spanning a range between 3.5 - 25 kppm. We acquire data for ≈ 600 sec per humidity level and select sections of these intervals according to their quality. The mean δ values of these sections are plotted as red and blue circles for δD and $\delta^{18}\text{O}$ respectively at the bottom part of figure 5. The points are fitted with a 3rd order polynomial plotted in black. Error bars refer to $\pm 1\sigma$ as calculated separately for every section. At the top of figure 5 we present the water levels of a concatenated series of the different sections used.

From the fitted curves in figure 5 we observe an overall linear response of $\delta^{18}\text{O}$ to different water levels. This is however not the case for δD , which shows a strong non-linearity at the low humidity area. For both isotopologues, the uncertainty of the measurement shows a rapid increase below 5000 ppm. In order to correct our measurements for possible fluctuations of the injected water sample, we focus on the linear response area between 15 - 22 kppm. A linear fit on the data, is presented in figure 6. For each data point the correction term $\Delta\delta_{hum}$ will be given by:

$$\Delta\delta_{hum} = \lambda \cdot (R_{20} - 1) \quad (8)$$

Where $R_{20} = \frac{[\text{H}_2\text{O}]_{ppm}}{20000_{ppm}}$ and λ is estimated from the linear regression:

$$\lambda_{18} = 1.94 \text{ ‰} \quad \lambda_D = 3.77 \text{ ‰} \quad (9)$$

So for a deviation of 1000 ppm

$$\Delta\delta^{18}\text{O} = 0.097 \text{ ‰} \quad \Delta\delta\text{D} = 0.19 \text{ ‰} \quad (10)$$

Brand et al (10) have performed a similar calibration using water samples injected in a discrete mode with a commercially available sample preparation line that consists of an autosampler and a liquid vaporizer (21). A comparison of the two data sets and the calibration lines shows a good agreement over the whole range of humidities.

C. Memory effects

The continuous flow of liquid and gaseous sample in the transfer lines, the evaporation chamber and the optical cavity of the spectrometer result in apparent dispersion effects. These effects impose a cross talk between samples commonly referred to as “memory effects”. In the case of isotopic analysis performed in a discrete mode the memory effect influencing the j^{th}

analysis of the run depends on the isotopic value of the n previous analyses weighted by a set of memory coefficients. So, if the expected value for the j^{th} analysis is δ_j^r and the measured equivalent is δ_j^m , then the memory effect M_j is described as:

$$\delta_j^r = \delta_j^m + M_j$$

$$M_j = \sum_{k=1}^n \varphi_k (\delta_j - \delta_{j-k}) \quad (11)$$

Determination of the memory coefficients is used to characterize the experimental system and to correct the measured isotopic values for observed memory effects.

In the case of continuous measurements we follow a slightly different approach. We generate an isotopic step by switching between two standard waters with different isotopic composition. This results in a smoothed sigmoid curve (figure 7). Ideally, in the case of zero dispersion, a switch between two standards would be described by a scaled and shifted version of the Heaviside unit step function as:

$$S(t) = \begin{cases} C_2 & t < 0 \\ C_1 H(t) + C_2 & t \geq 0 \end{cases} \quad (12)$$

where the valve switch takes place at $t = 0$, $H(t)$ is the Heaviside unit step function and C_1 and C_2 refer to the amplitude and base line level of the isotopic step. The effect of smoothing can be seen as the convolution of $S(t)$ with a smoothing function \mathcal{G} .

$$m(t) = [S * \mathcal{G}](t) \quad (13)$$

where $m(t)$ is the measured signal. The derivative of the signal $\frac{dm}{dt}$ yields the impulse response of the system as:

$$\frac{dm}{dt} = \frac{dS}{dt} * \mathcal{G} = C_1 \frac{dH}{dt} * \mathcal{G} = C_1 \delta_{Dirac} * \mathcal{G} \quad (14)$$

We fit the obtained data with a scaled version of the cumulative distribution function of a Log-Normal distribution described as

$$\delta_{model}(t) = \frac{K_1}{2} \left[1 + \operatorname{erf} \left(\frac{\ln t - t_{valve}}{S\sqrt{2}} \right) \right] + K_2 \quad (15)$$

where we estimate values for K_1 , K_2 , t_0 and S by means of a least square optimization (figure 7). The fit parameters are used to normalise the isotopic step. Based on the latter we then calculate the impulse response of the system as described in Eq. 14. As $t = t_{valve} = 0$ we consider the time at which the normalised step is equal to 0.5 and accordingly normalise the time scale (figure 8). The impact of the memory effects on the impulse response is visualised as the ratio $\mathcal{R}(t)/\mathcal{R}(t=0)$, calculated for $t \geq 0$ (figure 9). One can see that 40 sec after the introduction of the δ_{Dirac} pulse its effect

on the measured signal is below 10%. Beyond that point the noise level of the measurement does not allow for any conclusions regarding the memory effects.

D. Runs with 4 standards - VSMOW Calibration

Reporting of water isotopic measurements requires a proper calibration of the results on the VSMOW scale. This, in combination with the observed instrumental drift, implies the necessity for a frequent VSMOW calibration. In the following experiment we inject 5 samples of different isotopic composition spanning a range from -9‰ to -54‰ for $\delta^{18}\text{O}$ (-60‰ to -428‰ for δD). The set of samples consists of Copenhagen de-ionised water (CPH-DI) and a selection of 4 local standards. The latter's isotopic composition has been precisely measured with respect to VSMOW and SLAP waters on an IRMS with a high temperature conversion system (HTC). The water delivery is tuned to 19000 ppm well within the linear response area. During the whole run (≈ 2 h), humidity levels varied with a $\sigma_{[\text{H}_2\text{O}]} = 617$ ppm.

The raw data of the experiment are presented in figure 10. Before any further processing, a humidity calibration of the data is performed by scaling all data points to the level of 20000 ppm in the same fashion as described in the previous section. We choose sections of 35 data points (≈ 4 min) for every separate injection of a sample. Based on two of those sections and in combination with the values obtained by the HTC system we calculate the coefficients of a VSMOW calibration line as described by:

$$\delta_{\text{VSMOW}} = a_{\text{VSMOW}} \cdot \delta_{\text{measured}} + b_{\text{VSMOW}} \quad (16)$$

The sections are carefully selected in order to exclude data affected by memory effects occurring for some seconds after the valve switch between samples. The results of the measurements are presented in table I. The final values are compared to the values of the samples as measured on the HTC mass spectrometer system. The overall precision of the system for δD and $\delta^{18}\text{O}$ is below 0.5 ‰ and 0.1 ‰ respectively. The average of the differences between the CFA - CRDS and the HTC system is -0.05 ‰ for $\delta^{18}\text{O}$ and -0.42 ‰ for δD .

V. CONCLUSIONS AND OUTLOOK

We have demonstrated the feasibility of on-line liquid water isotopic measurements by interfacing a low volume continuous stream flash evaporator to a Cavity Ring Down Infra Red spectrometer. We have assessed the performance of the system regarding precision, accuracy,

possible instrumental drifts, memory effects and dependancy on varrying humidity levels. The observed instrumental drifts are minimal, thus allowing for reasonable sampling times. Additionally, the humidity dependance of the system is easily corrected via a careful and repeatable calibration procedure.

We have also indicated a procedure to calibrate the measured isotopic ratios on the VSMOW scale using local standard waters. The system's precision is comparable to that of modern mass spectrometry measurement systems tailored for water isotope analysis.

The use of the system is oriented towards the area of high resolution on-line continuous isotopic analysis of ice cores. The low power consumption and portability, offer the possibility for field operation. The proposed calibration technique can be performed in ≈ 30 min, it requires a small amount of water (≈ 2 -3 ml per standard) and can in principle be automated. Dispersion and memory effects are expected to smooth the acquired signals thus reducing the resolution that can be obtained with this technique. Consequently a careful determination of the systems resolution is essential as a next step towards continuous ice core measurements. Further reduction of the volume of the transfer lines prior to the optical cavity can potentially improve the system to that end.

ACKNOWLEDGEMENTS

We would like to thank Professor Dorth Dahl-Jensen for her support in our work. Jim White and Bruce Vaughn have contributed to this work with valuable comments and discussions. We would also like to thank Aaron van Pelt for his assistance during this project. This work was partly funded by the Marie Curie RTN "Network for Ice Sheet and Climate Evolution", MRTN-CT-2006-036127

REFERENCES

- [1] T. Epstein S. Mayeda, *Variations of ^{18}O content of waters from natural sources.*, *Geochimica Cosmochimica Acta* 4 (1953), p. 213224.
- [2] J. Bigeleisen, M.L. Perlman, and H.C. Prosser, *Conversion Of Hydrogenic Materials To Hydrogen For Isotopic Analysis*, *Analytical Chemistry* 24 (1952), pp. 1356–1357.
- [3] B.H. Vaughn, J.W.C. White, M. Delmotte, M. Troler, O. Cattani, and M. Stievenard, *An automated system for hydrogen isotope analysis of water*, *Chemical Geology* 152 (1998), pp. 309–319.
- [4] M. Gehre, R. Hoefling, P. Kowski, and G. Strauch, *Sample preparation device for quantitative hydrogen isotope analysis using chromium metal*, *Analytical Chemistry* 68 (1996), pp. 4414–4417.
- [5] I.S. Begley and C.M. Scrimgeour, *High-precision $\delta^2\text{H}$ and $\delta^{18}\text{O}$ measurement for water and volatile organic compounds by continuous-flow pyrolysis isotope ratio mass spectrometry*, *Analytical Chemistry* 69 (1997), pp. 1530–1535.
- [6] M. Gehre, H. Geilmann, J. Richter, R.A. Werner, and W.A. Brand, *Continuous flow $^2\text{H}/^1\text{H}$ and $^{18}\text{O}/^{16}\text{O}$ analysis of water samples with dual inlet precision*, *Rapid Communications In Mass Spectrometry* 18 (2004), pp. 2650–2660.
- [7] E.R.T. Kerstel, R. Trigvnan, N. Dam, J. Reuss, and H.A.J. Meijer, *Simultaneous determination of the $^2\text{H}/^1\text{H}$, $^{17}\text{O}/^{16}\text{O}$ and $^{18}\text{O}/^{16}\text{O}$ isotope abundance ratios in water by means of laser spectrometry*, *Analytical Chemistry* 71 (1999), pp. 5297–5303.
- [8] R.Q. Iannone, S. Kass, H.J. Jost, M. Chenevier, D. Romanini, H.A.J. Meijer, S. Dhaniyala, M. Snels, and E.R.T. Kerstel, *Development and airborne operation of a compact water isotope ratio infrared spectrometer*, *Isotopes in Environmental and Health Studies* (2009), pp. —.
- [9] G. Lis, L.I. Wassenaar, and M.J. Hendry, *High-precision laser spectroscopy D/H and O-18/O-16 measurements of microliter natural water samples*, *Analytical Chemistry* 80 (2008), pp. 287–293.
- [10] W.A. Brand, H. Geilmann, E.R. Crosson, and C.W. Rella, *Cavity ring-down spectroscopy versus high-temperature conversion isotope ratio mass spectrometry; a case study on $\delta^2\text{H}$ and $\delta^{18}\text{O}$ of pure water samples and alcohol/water mixtures*, *Rapid Communications in Mass Spectrometry* 23 (2009), pp. 1879–1884.
- [11] L.X. Wang, K.K. Caylor, and D. Dragoni, *On the calibration of continuous, high-precision delta O-18 and delta H-2 measurements using an off-axis integrated cavity output spectrometer*, *Rapid Communications In Mass Spectrometry* 23 (2009), pp. 530–536.
- [12] X.H. Lee, S. Sargent, R. Smith, and B. Tanner, *In situ measurement of the water vapor O-18/O-16 isotope ratio for atmospheric and ecological applications*, *Journal Of Atmospheric And Oceanic Technology* 22 (2005), pp. 555–565.
- [13] R.Q. Iannone, D. Romanini, S. Kass, H.A.J. Meijer, and E.R.T. Kerstel, *A Microdrop Generator for the Calibration of a Water Vapor Isotope Ratio Spectrometer*, *Journal Of Atmospheric And Oceanic Technology* 26 (2009), pp. 1275–1288.
- [14] H. Ulmke, T. Wriedt, and K. Bauckhage, *Piezoelectric droplet generator for the calibration of particle-sizing instruments*, *Chemical Engineering & Technology* 24 (2001), pp. 265–268.

- [15] J. Morville, S. Kassi, M. Chenevier, and D. Romanini, *Fast, low-noise, mode-by-mode, cavity-enhanced absorption spectroscopy by diode-laser self-locking*, Applied Physics B-Lasers And Optics 80 (2005), pp. 1027–1038.
- [16] E.R.T. Kerstel, R.Q. Iannone, M. Chenevier, S. Kassi, H.J. Jost, and D. Romanini, *A water isotope (^2H , ^{17}O , ^{18}O) spectrometer based on optical feedback cavity-enhanced absorption for in situ airborne applications*, Applied Physics B-Lasers And Optics 85 (2006), pp. 397–406.
- [17] K. Fuhrer, A. Neftel, M. Anklin, and V. Maggi, *Continuous Measurements Of Hydrogen-Peroxide, Formaldehyde, Calcium And Ammonium Concentrations Along The New Grip Ice Core From Summit, Central Greenland*, Atmospheric Environment Part A-General Topics 27 (1993), pp. 1873–1880.
- [18] P.R. Kaufmann, U. Federer, M.A. Hutterli, M. Bigler, S. Schupbach, U. Ruth, J. Schmitt, and T.F. Stocker, *An Improved Continuous Flow Analysis System for High-Resolution Field Measurements on Ice Cores*, Environmental Science & Technology 42 (2008), pp. 8044–8050.
- [19] S. Schüpbach, U. Federer, P.R. Kaufmann, M.A. Hutterli, D. Buiron, T. Blunier, H. Fischer, and T.F. Stocker, *A New Method for High-Resolution Methane Measurements on Polar Ice Cores Using Continuous Flow Analysis*, Environmental Science & Technology 43 (2009), pp. 5371–5376.
- [20] E.R.T. Kerstel, *Isotope ratio infrared spectrometry*, in *Handbook of Stable Isotope Analytical Techniques* P. de Groot ed., , Vol. 1 Elsevier B.V., 2005, chap. 34, pp. 759–787.
- [21] P. Gupta, D. Noone, J. Galewsky, C. Sweeney, and B.H. Vaughn, *Demonstration of high-precision continuous measurements of water vapor isotopologues in laboratory and remote field deployments using wavelength-scanned cavity ring-down spectroscopy (WS-CRDS) technology*, Rapid Communications In Mass Spectrometry 23 (2009), pp. 2534–2542.
- [22] E.R. Crosson, *A cavity ring-down analyzer for measuring atmospheric levels of methane, carbon dioxide, and water vapor*, Applied Physics B-Lasers And Optics 92 (2008), pp. 403–408.
- [23] G. Berden, R. Peeters, and G. Meijer, *Cavity ring-down spectroscopy: Experimental schemes and applications*, International Reviews In Physical Chemistry 19 (2000), pp. 565–607.
- [24] P. Werle, R. Mucke, and F. Slemr, *The Limits Of Signal Averaging In Atmospheric Trace-Gas Monitoring By Tunable Diode-Laser Absorption-Spectroscopy (Tdlas)*, Applied Physics B-Photophysics And Laser Chemistry 57 (1993), pp. 131–139.
- [25] F. Czerwinski, A.C. Richardson, and L.B. Oddershede, *Quantifying Noise in Optical Tweezers by Allan Variance*, Optics Express 17 (2009), pp. 13255–13269.
- [26] D.W. Allan, *Statistics of atomic frequency standards*, Proceedings of the IEEE 54 (1966), pp. 221–230.

Sample ID	δD [‰]	$\bar{\delta} D$ Span	δD_{HTC} $\delta D_{HTC} - \bar{\delta} D$
CPH-DI	-60.33	-60.26	-
CPH-DI	-60.18	0.1	-
-22	-167.66	-168.03	-168.4
-22	-168.40	0.52	-0.37
Crete	-260.70	-260.94	-261.9
Crete	-261.19	0.34	-0.96
-40	-309.13	-309.57	-310
-40	-310.00	0.62	-0.44
DC02	-427.31	-427.58	-427.5
DC02	-427.85	0.38	0.08
Std. dev all			0.39
$\delta D_{HTC} - \bar{\delta} D$ all			-0.42
Sample ID	$\delta^{18}O$ [‰]	$\bar{\delta}^{18}O$ Span	$\delta^{18}O_{HTC}$ $\delta^{18}O_{HTC} - \bar{\delta}^{18}O$
CPH-DI	-8.69	-8.70	-
CPH-DI	-8.70	0.01	-
-22	-21.9	-21.92	-21.9
-22	-21.93	0.02	0.02
Crete	-33.57	-33.54	-33.64
Crete	-33.52	0.04	-0.1
-40	-39.69	-39.83	-39.97
-40	-39.98	0.2	-0.14
DC02	-54.08	-54.11	-54.08
DC02	-54.14	0.04	0.03
Std. dev all			0.06
$\delta^{18}O_{HTC} - \bar{\delta}^{18}O$ all			-0.05

TABLE I
RESULTS OF THE 4 STANDARDS EXPERIMENT

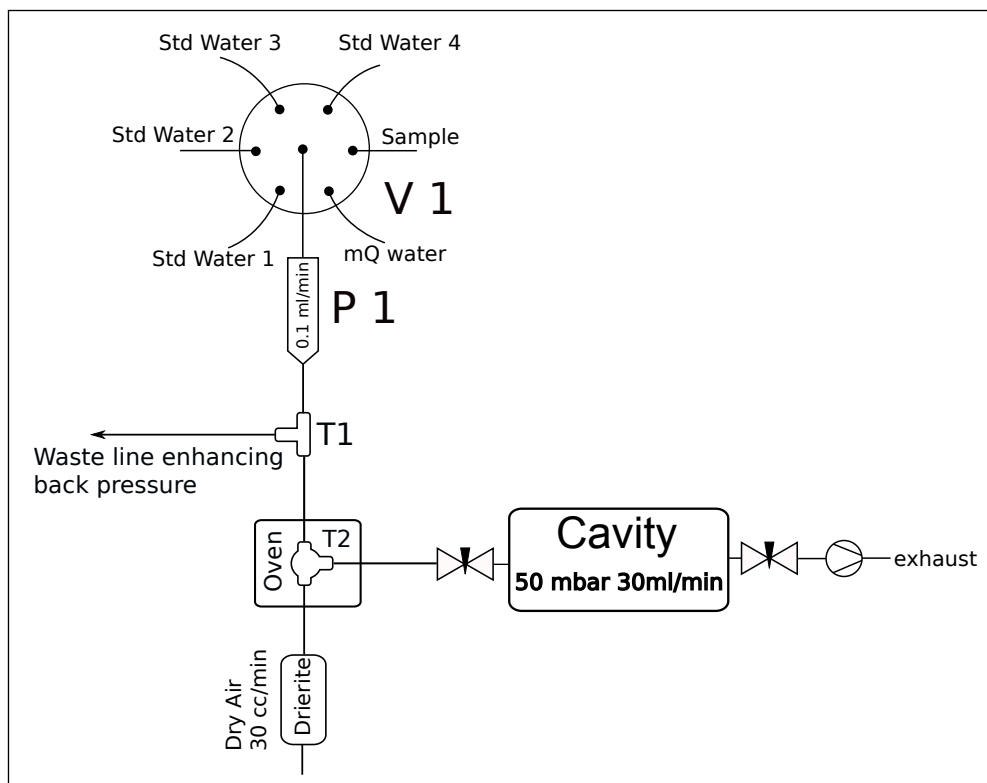


Fig. 1. Block diagram of the CFA-CRDS system

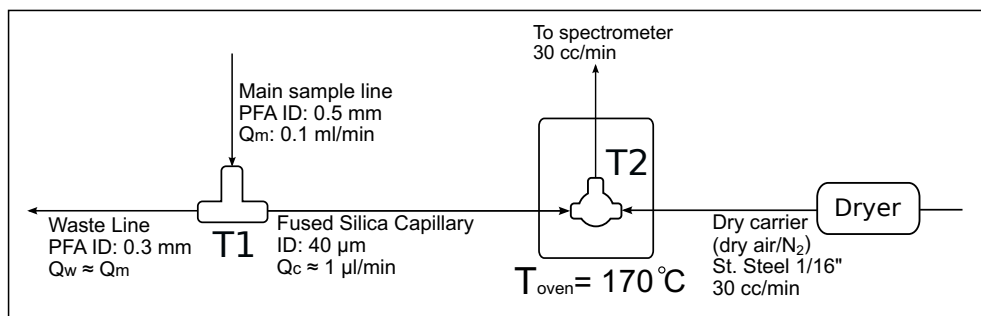


Fig. 2. Detailed section of the sample split

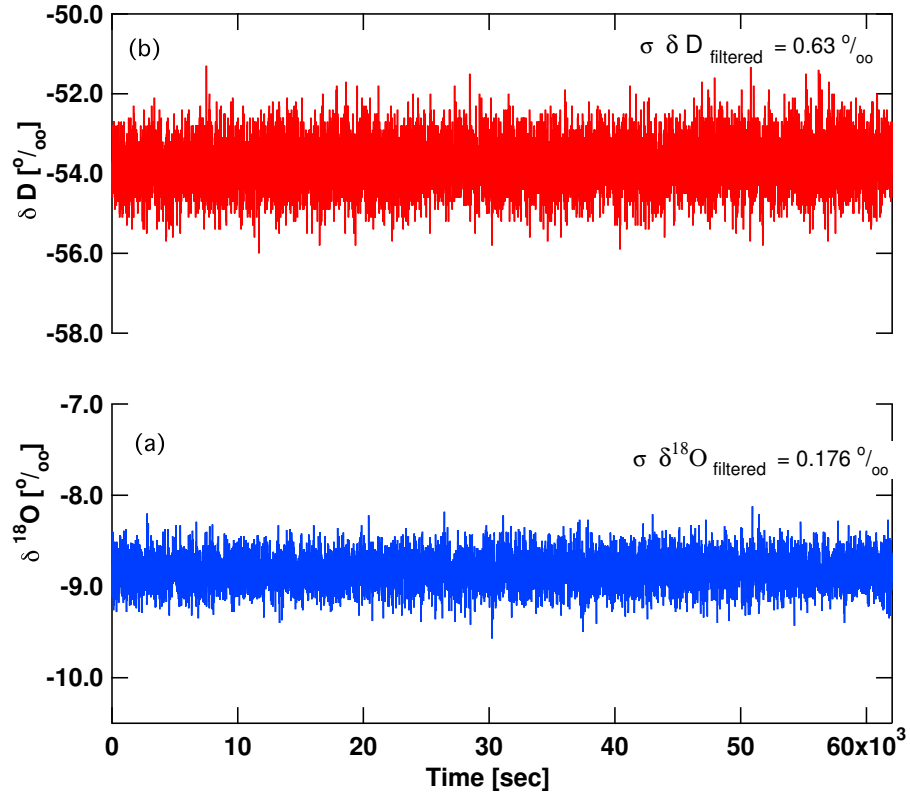


Fig. 3. Injection of de-ionized water over the period of 17 hours. Results for $\delta^{18}\text{O}$ (a) and δD (b)

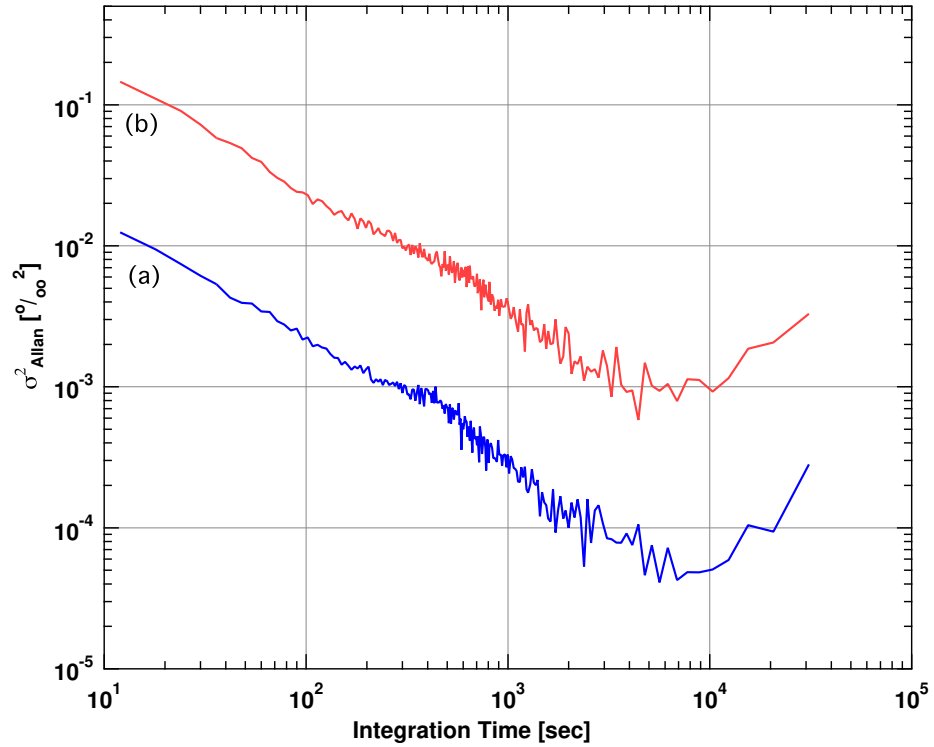


Fig. 4. Allan variance plots for $\delta^{18}\text{O}$ (a) and δD (b) from the data in figure 3.

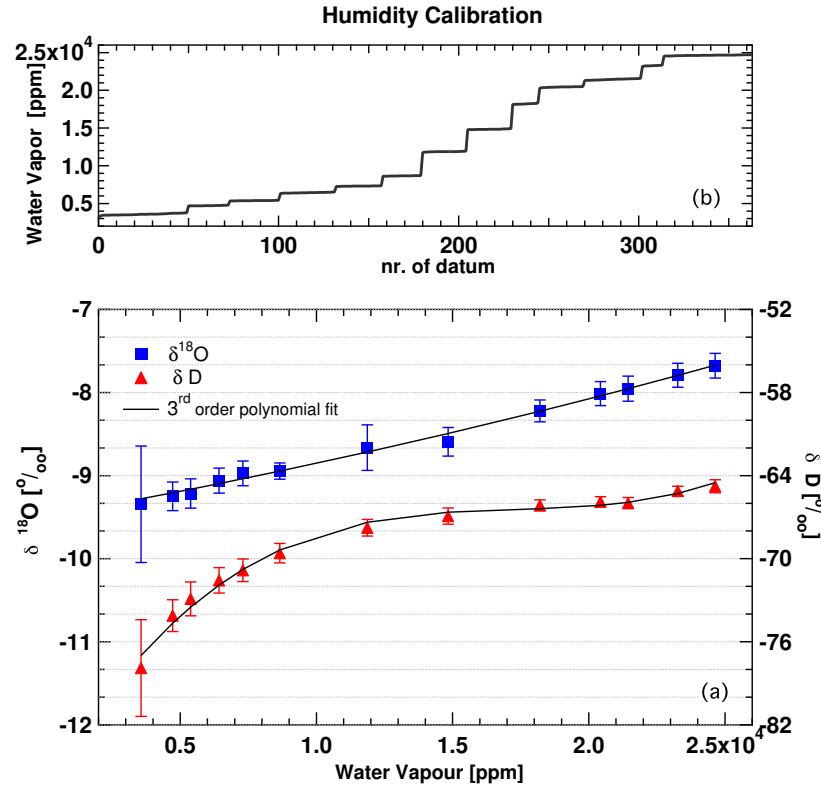


Fig. 5. Humidity calibration. The averages of the isotopic values for each section are plotted as blue squares for $\delta^{18}\text{O}$ and red triangles for δD in graph (a). Data are fitted with a 3rd order polynomial regression model (solid lines). The error bars represent $\pm 1\sigma$ of each processed section. In (b) we plot the humidity levels of each section.

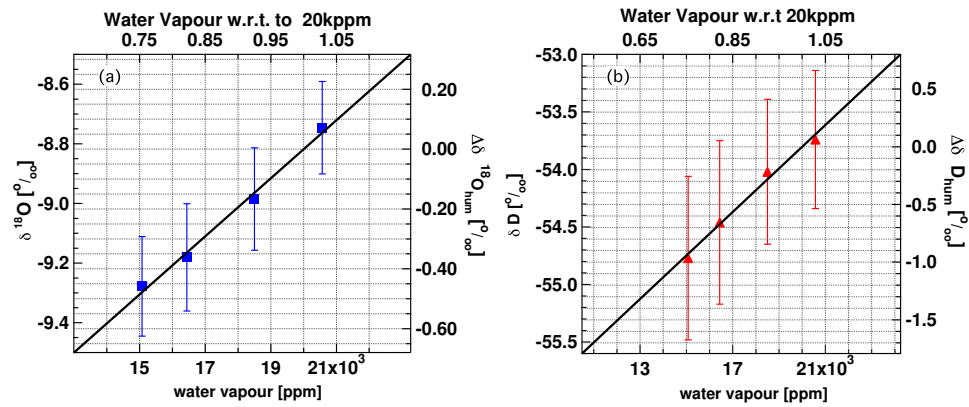


Fig. 6. The averages of each humidity level section are plotted as blue squares and red triangles for $\delta^{18}\text{O}$ and δD respectively. Error bars represent a $\pm 1\sigma$ of each section.

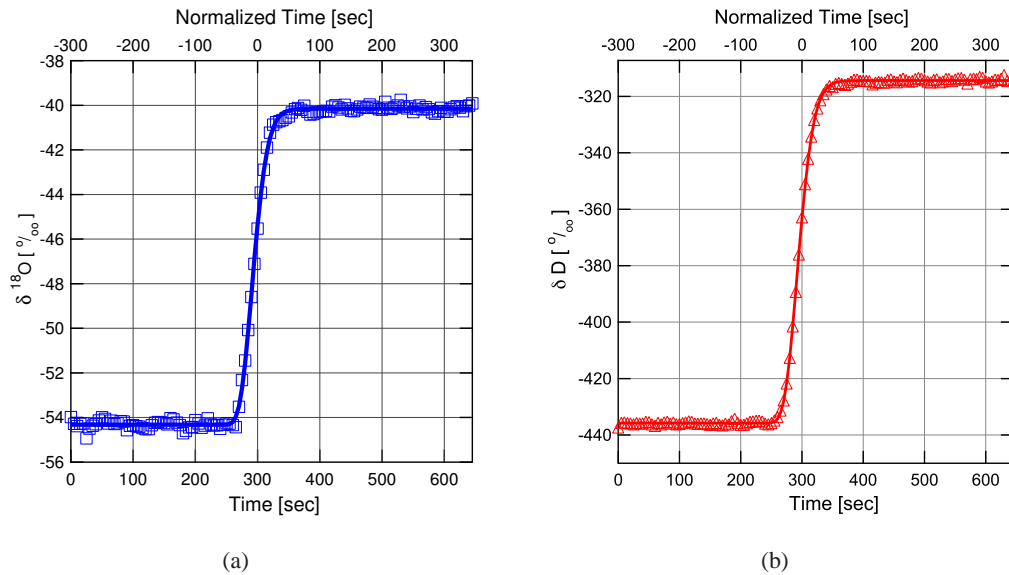


Fig. 7. Raw $\delta^{18}\text{O}$ and δD data during the valve switch between standard water “DC02” and “-40” are plotted with blue squares and red triangles respectively. We fit a Log Normal distribution model plotted with blue (a) for $\delta^{18}\text{O}$ and red (b) for δD ..

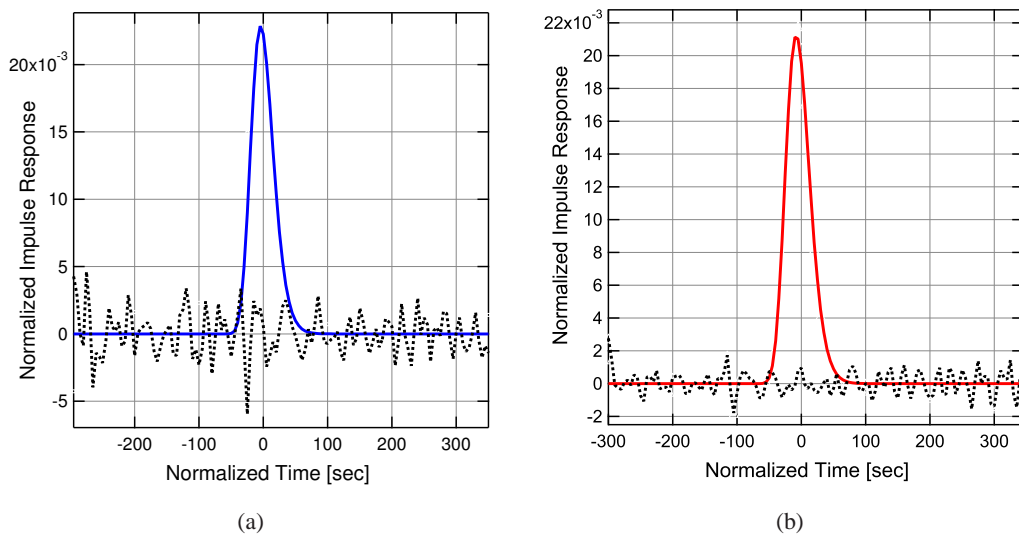


Fig. 8. Response of the system on an isotopic δ_{Dirac} pulse for $\delta^{18}\text{O}$ (blue curve) and δD (red curve) introduced at $t = 0$. The dotted lines represent the residuals of the fit.

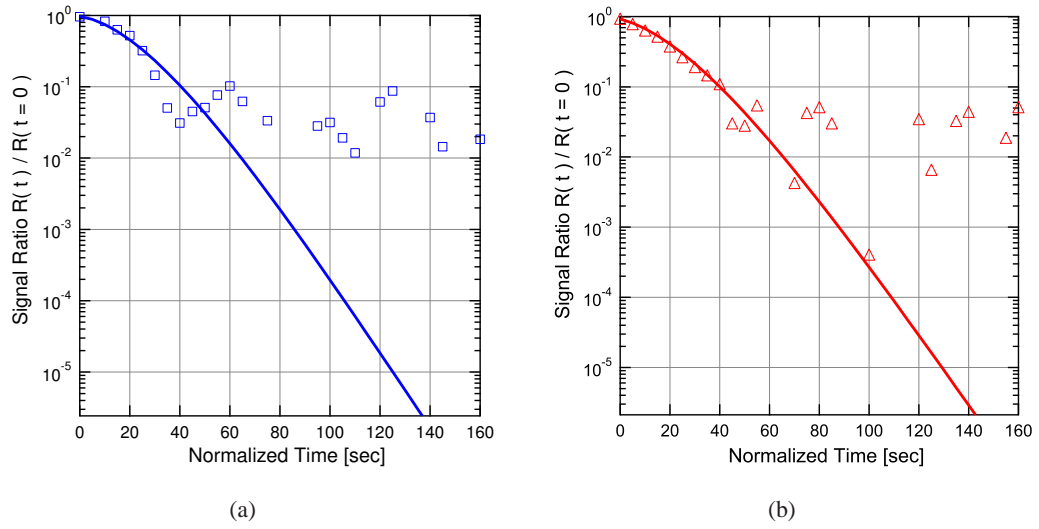


Fig. 9. Quantification of the memory effect for $\delta^{18}\text{O}$ (a) and δD (b). $R(t)$ refers to the amplitude of the impulse response of the system at time t .